



# Incorporation of tin in nanocrystalline CdSe thin films: a detailed study of optoelectronic and microstructural properties

Prashant K. Sahu<sup>1</sup> · R. Das<sup>1</sup> · Rajesh Lalwani<sup>1</sup>

Received: 17 July 2018 / Accepted: 5 September 2018 / Published online: 6 September 2018  
© Springer-Verlag GmbH Germany, part of Springer Nature 2018

## Abstract

Tin-doped nanocrystalline CdSe thin films were deposited onto glass substrate by simple chemical bath deposition technique. The films obtained were uniform and had good adherence to the substrate. The influence of Sn (0–5%) doping on the optical, photoluminescence, electrical, morphological, compositional and structural properties of the films was investigated. The optical absorption studies revealed that the optical band gap of the films varied from 2.62 eV for nano CdSe to 2.50 eV for 5% Sn:CdSe. These films are appropriate for application in different optoelectronics devices due to band gap tunability property. To analyze photoluminescence properties, the films were excited by UV (235 nm) and almost green spectrum was emitted by the films. It is observed that the low temperature resistivity of the thin films was in the range  $10^7$ – $10^4$   $\Omega$  cm and also found to decrease with Sn concentration, as resulted from the dc two probe measurements. Activation energy was also calculated. Noticeable changes were observed in the optical and electrical properties of CdSe thin films due to the presence of Sn dopant. Surface morphology study using TEM/SEM showed almost uniform distribution of spherical grains. The elemental composition study using energy dispersive spectroscopy (EDAX) confirms the existence of the desired elements. X-ray diffraction pattern indicated that the formed structure is cubic with most prominent peak at (111). Some important structural parameters such as lattice constant, crystallite size, strain, dislocation density and number of crystallites per unit area were calculated and presented.

## 1 Introduction

Two key factors cause the properties of nanomaterial to be special: their quantum effects and their structure. Their tiny structure means they have a greater relative surface area than other materials and this can alter or improve properties such as strength and electrical characteristics or reactivity. In recent years, major attention has been given for the preparation and examination of doped chalcogenide thin films such as CdS, CdSe, CdTe, etc., because of their brilliant semiconducting properties and applications. Out of these CdSe belongs to II–VI semiconductor group with direct band gap of 1.74 eV which is tunable [1] and due to its excellent optical and electrical properties it is a promising semiconducting material for many photovoltaic and

optoelectronic applications such as high efficiency solar cell, diode laser, nanosensors, light emitting diodes and other optoelectronic devices [1–6]. The nano dimensions of these thin films effects the band structure which changes the optical and electrical properties and that can be used as a new type of fluorescence materials and labelling materials for biological research by controlling the crystallite size [5]. The electrical and optical properties can also be tailored by appropriate doping [6].

With the different preparing methods, the diameter, phase structure, morphology uniformity, and properties are also different accordingly. Das et al. [7] have reported the effect of Sn doping on bulk CdS thin films with highly improved photoconductivity with a current gain of  $10^6$ . Recently SnSe semiconducting thin films have attracted researchers due to its variety of applications. The SnSe thin films with optical bandgaps of 0.95–1.14 eV were deposited by chemical bath deposition with thickness from 100 to 310 nm and having orthorhombic structure [8]. However, a recent research on high-quality epitaxial growth of SnSe films was studied using pulsed laser deposition with indirect optical band gap of 0.8 eV and direct band gap of 1.3 eV [9]. The structural,

✉ Prashant K. Sahu  
prashantsahu.2712@gmail.com

Rajesh Lalwani  
dwijendrad@yahoo.co.in

<sup>1</sup> Department of Applied Physics, Bhilai Institute of Technology, Durg, C.G. 491001, India

morphological, and optical properties of  $\alpha$ -SnSe thin films were investigated by changing Sn/Se ratio. The formation of single phase  $\alpha$ -SnSe was observed at a substrate temperature of 400 °C for selenium amount of 1.0 g [10]. The photovoltaic behavior of SnS and SnSe are examined using bulk heterojunction and photocurrent response [11]. SnSe thin films of thickness 180 nm have been deposited on glass substrates by reactive evaporation at an optimized substrate temperature of  $523 \pm 5$  K and pressure of 10 mbar [12]. Structural, morphological, optical and sensing properties of SnSe and SnSe<sub>2</sub> thin films as a gas sensing material are examined [13]. Kaur et al. [14–16] deposited Sn-doped CdSe on glass substrate by thermal evaporation method in an argon gas atmosphere. They reported that films are hexagonal in nature and a red shift of the absorption edge was observed with annealing. They also reported increase in refractive index, optical conductivity and dielectric constants after annealing. Dhanasekaran et al. [17] have deposited nanocrystalline Cd<sub>x</sub>Sn<sub>1-x</sub>Se thin films ( $x = 1, 0.7, 0.45, \text{ and } 0$ ) by electrodeposition technique. They showed that how the band gap can be varied by doping with Sn and can be utilized for optoelectronics applications. Thin films of CdSnSe have been developed on transparent conducting oxide (TCO) coated glasses by electrolytic deposition [18]. The film that was obtained from 10 g/l of Sn in the bath, showed an optimum spectral sensitivity. The optical band gap energy of bulk CdSnSe thin films is found to be in the range of 1.23–1.25 eV [19]. The literature survey revealed that no reports are available on preparation of Sn-doped CdSe nanoparticle thin film by simple chemical method. In the present study, tin doped CdSe thin films (Sn:CdSe) at different contents (0–5 wt%) were deposited onto glass substrates by chemical bath deposition method at room temperature. The samples were characterized by Optical absorption, photoluminescence, SEM, EDAX, XRD and electrical techniques. The structural, optical and electrical, as well as surface wettability properties were extensively studied and reported.

## 2 Experimental details

### 2.1 Deposition of CdSe and Sn:CdSe thin films

Thin films of undoped and Sn-doped nanocrystalline CdSe were deposited on commercial glass slides of size 75 × 25 mm using chemical bath deposition technique. Before deposition, they were immersed in nitric acid for a period of 48 h to obtain a clean and contamination-free glass surface. After that the slides were washed with detergent and finally cleaned in ultrasonic cleaner with triple distilled water for 15 min and then dried in air for the formation of nucleation centers. To deposit films at room temperature 100 ml beaker was taken and reactive bath solution was

prepared by mixing aqueous solutions of 10 ml (0.5 M) cadmium acetate, 10 ml (30%) ammonia, 5 ml triethanolamine and freshly prepared and filtered 15 ml (0.5 M) sodium selenosulphate. Using reflux condenser along with magnetic stirrer attached with the hot plate, sodium selenosulphate solution was prepared just prior to deposition by dissolving selenium pellets in a sodium sulfite solution at 80 °C with stirring for a period of 5 h. The high purity (99.99%) selenium pellets and chemicals of AR grade (Sigma Aldrich) were used here. For Sn doping (0.5 M) stannous chloride solution was added to the bath with different proportions. Then glass slides were immersed in the beaker vertically. Ammonia solution was used to maintain pH of the solution at  $11 \pm 0.3$  and complexing agent triethanolamine was used to increase the adherence of the films. Different parameters were optimized to obtain good quality films and reported in our earlier work [20]. Poor quality deposition was found for less duration and at high temperature hence was not continued and low temperature deposition at  $35 \pm 1$  °C was selected to avoid cracks in the films. After deposition of 24 h, the glass slides were taken out from beakers and thoroughly washed with triple distilled water followed by drying in the air at room temperature. A series of films were prepared for different concentrations of Sn from 0 to 5 at% and checked for optimal results.

### 2.2 Characterizations

Optical absorption and transmission spectra of the films were obtained at room temperature in the wavelength range of 400–800 nm using UV–Vis–NIR double beam spectrophotometer CHEMITO SPECTRASCAN-2600. The photoluminescence spectra of the films were taken using a constant deviation spectrometer in the visible range 400–700 nm. UV source with filters from 235 to 320 nm was used as excitation source. A photomultiplier tube (RCA931A), was used to detect emitted light and finally the emitted light output was recorded in the form of current using digital Pico-ammeter (DPM-121, SES, Roorkee, India). SES-CAMM computer aided measurement module for Two Probe Experiment, TPX-1.1 (Scientific Instruments, Roorkee) was used to study the variation of electrical resistivity with temperature. Contact angle measurements were carried by high precision travelling microscope with least count 0.001 cm. High-resolution transmission electron microscopy (HRTEM) images were obtained using a JEOL/JEM-2100 electron microscope operated at an accelerating voltage of 200 kV. Surface morphology was examined by scanning electron microscope (SEM) JEOL JSM-5600. Elemental study was carried out using EDS (INCA Oxford) coupled with SEM. Structural characterization of the samples was carried out using D8 Advance diffractometer with CuK $\alpha$  line (wavelength = 1.54060 Å) in 2 $\theta$  range from 20° to 70° in a step of

0.02°. Raman spectra were recorded by Jobin Yvon Horibra LABRAM HR-800 in the range 100–780 cm<sup>-1</sup> at room temperature. (25 mW) diode laser with wavelength 473 nm was used for excitation and scanning time was 100 s.

### 3 Results and discussion

Films prepared by this method were dark orange in color, smooth, uniform, physically hard and strongly fixed to the substrate support. The thickness of the films was measured by weight difference method using highly sensitive Shimadzu micro balance (0.1 mg). It is in the range of 280 nm for undoped CdSe and 302 nm, 370 nm and 384 nm for 1%, 3% and 5% Sn:CdSe thin films.

#### 3.1 Optical properties

The absorption coefficient is an important optical parameter which defines how much light of a given color (or wavelength) will be absorbed by a material of a given thickness. Basically, it describes the amount of light absorbed per thickness of material. If a material absorbs more light, its absorption coefficient will be higher. Figure 1 presents the plots of absorbance and absorption coefficient with wavelengths which shows the exponential decay with increasing wavelength. It can be seen here that overall variation and shapes of the curves are nearly identical, but values observed are slightly different. For higher wavelength region

all films show lower absorption while it increases sharply for lower wavelengths. The absorption coefficient was found to increase with Sn doping, which may be due to increase in thickness and crystallite size. Generally, in thicker films more atomic states are present which are responsible for the absorption of photon energy, hence absorbance and absorption coefficient increase here [21].

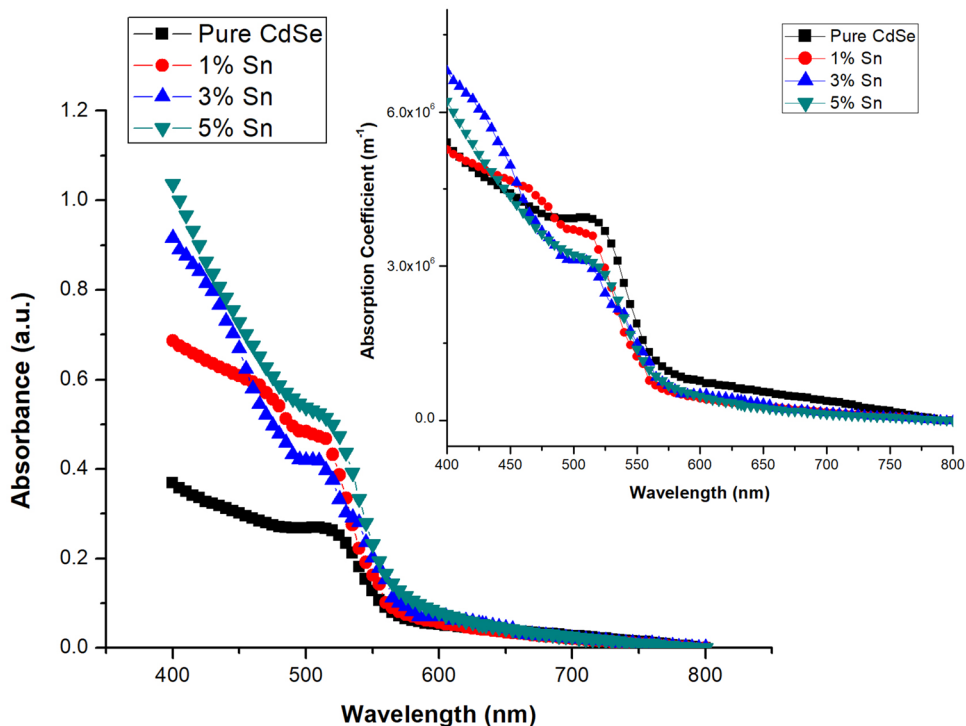
Absorption coefficient ( $\alpha$ ) of the films is calculated using relation

$$\alpha = \frac{2.302 \cdot A}{t} \text{ or } \alpha = \frac{1}{t} \ln\left(\frac{1}{T}\right) \tag{1}$$

where  $A$  is absorbance,  $T$  is transmittance, and  $t$  is film thickness. Higher values of  $\alpha > 10^6 \text{ m}^{-1}$  may correspond to a transition taking place between extended states in both conduction and valance bands, while region with lower values of  $\alpha$  shows rough exponential behavior [22]. For lower wavelength between 400 and 450 nm the measured values of  $\alpha$  is maximum for 3% and 5% Sn:CdSe thin films as compared to 1% Sn:CdSe and undoped CdSe thin films. 3% and 5% Sn:CdSe thin films give highest absorption coefficient, therefore, more solar energy spectrum can be used here which also indicates that these are superior over others.

Prepared films showed high absorption coefficient in near UV region that decreased exponentially towards the NIR region. This property of having high absorption coefficient in the near UV region make the films good for screening off UV portion of electromagnetic spectrum which is unsafe to human.

**Fig. 1** Absorbance spectra of undoped and Sn doped CdSe thin films (with different doping percentages)



After comparison, the size quantization effects of nanoparticles of undoped CdSe and (1%, 3%, 5%) Sn: CdSe were studied for maximum steep rise in absorption. The absorption data was analyzed, and the band gap of the films was determined using classical Tauc relation [21]

$$(\alpha h\nu)^{1/n} = A(h\nu - E_g) \tag{2}$$

where  $A$  is a constant,  $E_g$  is band gap and  $n$  is constant which depends on the type of transition. To estimate the type of transitions, plot of  $(\alpha h\nu)^2$  versus  $h\nu$  is shown in Fig. 2. Direct transition can be observed here as the nature of the graph is linear hence the value of  $n$  has been taken as  $1/2$  for allowed direct transition. The value of band gap  $E_g$  was calculated by extrapolating the straight line on  $x$ -axis whose intercept on  $x$ -axis gives the band gap.

The observed optical band gap values are 2.62–2.50 eV and listed in Table 1. The value is quite high when compared with reported values (2.25, 1.83, 1.25, 1.68) eV in the literature [16, 17, 19, 23]. The variation in band-gap energy may be due to variation in grain structure and size of the Sn: CdSe crystallite. Calculated band gap values ( $E_g$ ) are higher than the optical band gap  $E_{g(\text{bulk})}$  of bulk CdSe which is around 1.74 eV at room temperature [24], showing blue shift. It was observed that the value of band gap decreases with Sn doping. In fact, the increase of the doping density causes the broadening of the intragap impurity bands. In particular, when the density of  $n$ -type or  $p$ -type doping becomes sufficiently high, the impurity band merges with the conduction or valence band and causes the formation of band tail and band gap shrinkage [6, 16]. Upon Sn doping, reduction in band gap increases optical

**Table 1** Values of band gap ( $E_g$ ), refractive index ( $n$ ), size of crystallites ( $D$ ) calculated from UV–Vis data

Films	Band gap ( $E_g$ ) (eV)	Band gap shift (eV)	$D$ (nm)	Refractive index ( $n$ )
CdSe	2.62	0.88	3.307	2.471
1% Sn: CdSe	2.59	0.85	3.365	2.481
3% Sn: CdSe	2.54	0.80	3.469	2.498
5% Sn: CdSe	2.50	0.76	3.559	2.513

absorbance and absorption coefficient (shown in Fig. 1). The refractive index provides many important information of the films like film density, cavities present in the film, speed of light in films, etc. It was calculated using Herve–Vandamme Formula [25] and listed in Table 1.

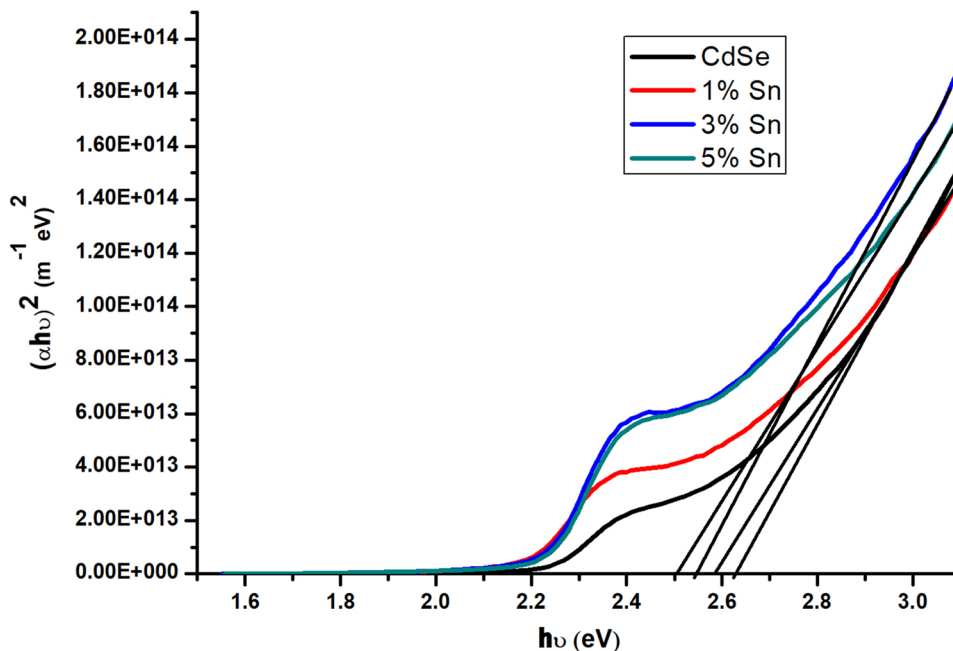
$$n^2 = 1 + \left( \frac{A}{E_g + B} \right)^2 \tag{3}$$

Here  $A$  and  $B$  are constants having values of 13.6 eV and 3.4 eV and  $E_g$  is the band gap [25]. Our results are comparable as observed by Kaur et al. [16]. Usually refractive index represents the density of the materials. Density of Sn (7.31 g/cm<sup>3</sup>) is higher than the density of CdSe (5.83 g/cm<sup>3</sup>); hence the increase in refractive index with Sn incorporation can be due to the increase in the density of the film.

The particle size was calculated using effective mass approximation Formula,

$$E_g = E_{g(\text{bulk})} + \frac{2\hbar^2\pi^2}{\mu D^2} \tag{4}$$

**Fig. 2** Plot of  $(\alpha h\nu)^2$  versus photon energy for the undoped CdSe and Sn doped CdSe thin films (with different doping percentages)



where  $D$  is the diameter of crystallites and  $\mu$  is the effective mass of electron–hole pair. The average size of nanocrystallites is calculated and listed in Table 1.

## 4 Raman spectra

The Raman spectra of undoped CdSe and 5% Sn:CdSe thin films is shown in Fig. 3. 25 mW diode laser was used as excitation source to take these spectra at room temperature. The measurement range was  $100\text{--}780\text{ cm}^{-1}$  with scanning time of 100 s. Two main peaks were obtained in both films related to first- and second-order longitudinal optical (LO) phonons modes. First and second LOs were detected at  $206.134\text{ cm}^{-1}$  and  $414.320\text{ cm}^{-1}$  for undoped CdSe thin films, whereas in 5% Sn:CdSe thin film we found the positions of first LO and second LO at  $207.496\text{ cm}^{-1}$  and  $415.646\text{ cm}^{-1}$ , respectively. Very small third LO was also spotted around  $613\text{ cm}^{-1}$ . The observed LO phonon frequency is very close to the standard bulk LO frequency ( $210\text{ cm}^{-1}$  and  $418\text{ cm}^{-1}$ ) [26], which confirms the formation of CdSe thin films. The Raman shift towards lower frequency in LO phonon frequency is basically due to the nanocrystalline nature and the strain developed in the films during deposition. Here peak is highest for undoped CdSe thin films because the optical band gap, i.e.,  $2.62\text{ eV}$  estimated from absorption data well matches with the excitation source energy ( $\lambda = 473$ , Energy =  $2.62\text{ eV}$ ).

## 4.1 Photoluminescence analysis

Photoluminescence study is a contactless, non-destroyable and authentic technique to investigate various optical properties. Figure 4 shows the PL emission spectra of Sn-doped CdSe thin films (with different percentages of Sn from 0 to 5%). To the best of our knowledge, literature on this is scarce.

An excitation wavelength of  $235\text{ nm}$  was selected for all samples out of various UV filters. All samples showed single peak which corresponds to free exciton emission which is close to the band–band transition. Figure 4 shows that the intensity increases with Sn doping, which may be due to the change in crystalline structure and increase in crystalline size. We got the emission peaks at  $500\text{ nm}$ ,  $515\text{ nm}$ ,  $523\text{ nm}$  and  $530\text{ nm}$  corresponding to green region for undoped CdSe, 1% Sn:CdSe, 3% Sn:CdSe and 5% Sn:CdSe thin films, respectively. Obtained values are very close to the results by Singh et al. [27] who observed green region ( $531\text{ nm}$ ) emission by CdSe thin films. These values are close to the band–band transition and electron–hole recombination involving levels in the band gap due to addition of impurities. F. Laatar et al. [28] have reported well defined PL peaks for CdSe thin films centered between  $546.2$  and  $552.35\text{ nm}$  because of deposition temperature. The position of the band–band PL emission of bulk CdSe is  $730\text{ nm}$  and comparison of this with our prepared samples, shows blue shift and strong quantum confinement. Small variations in the position of emission band with doping percentage are observed, which indicates that the lattice remains the

**Fig. 3** Raman Spectra of undoped CdSe and 5% Sn:CdSe thin films

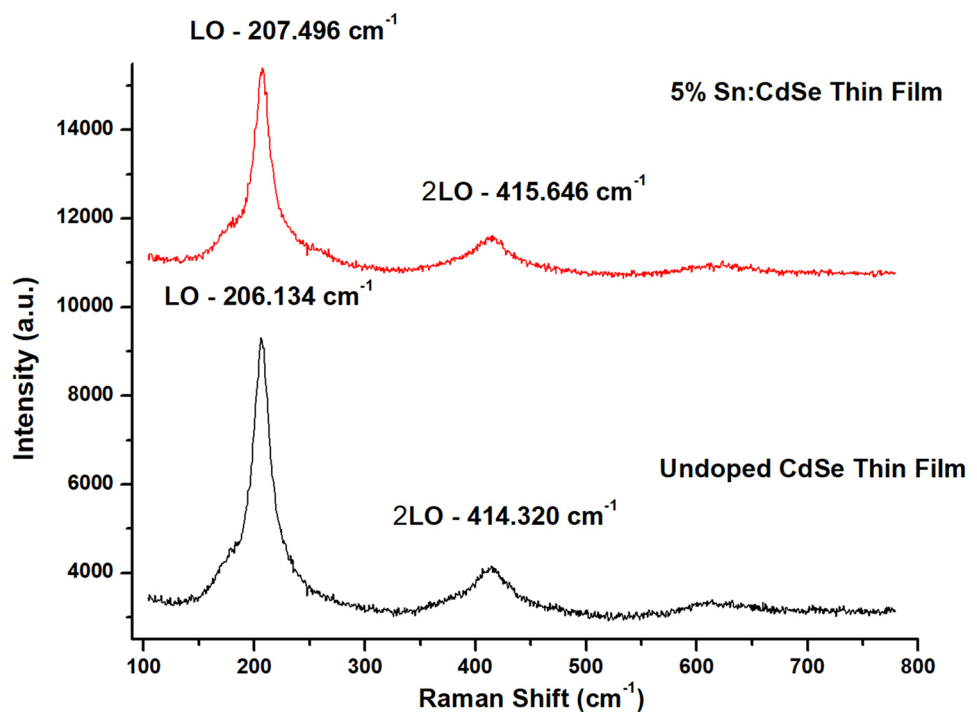
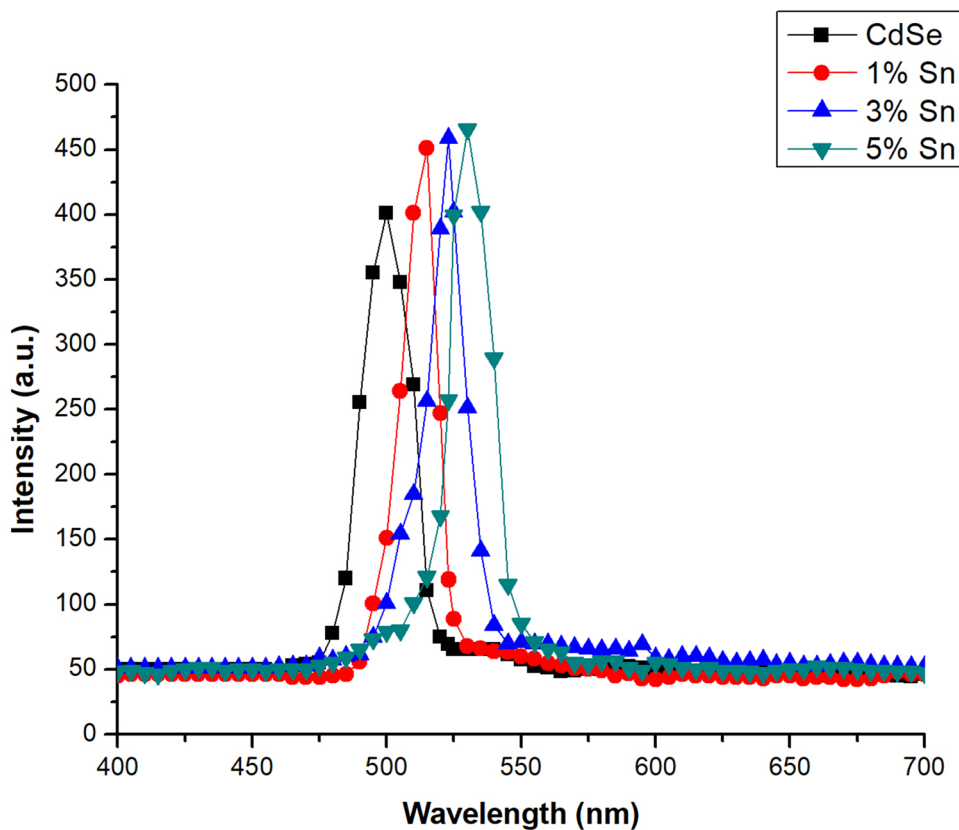


**Fig. 4** Photoluminescence emission spectra of undoped CdSe and Sn doped CdSe thin films at room temperature showing the variation in the intensity with respect to doping percentage



same [28]. Highest peak was observed for 5% Sn:CdSe thin films. Enhanced PL peaks is due to the presence of high surface state. As we know that nano size crystallite generally has high density of surface state due to large surface–volume ratio. These surface states may behave as traps for the photo excited carriers which increase luminescence [29]. PL spectra shows red shift with doping as decrease in the band gap was also observed. The Commission International del’Echairage (CIE) chromaticity coordination ( $x, y$ ) of the prepared films was calculated and shown in Fig. 5. The value of CIE coordinates of undoped CdSe thin film was calculated as (0.2550, 0.3886) corresponds to light blue region. Thus, it can be used as bluish phosphor. However, on Sn doping, we found these values as (0.2567, 0.4564), (0.2739, 0.4931) and (0.2780, 0.5101) for 1% Sn doped CdSe, 3% Sn doped CdSe and 5% Sn doped CdSe thin films, respectively. It is clear in the CIE chromaticity diagram that for 1% Sn-doped CdSe and 3% Sn-doped CdSe thin films spectra lie in the blue region with little green component. Similarly, for 5% Sn-doped CdSe thin film spectra lies in light green region.

Mostly phosphors are prepared by doping rare earth elements which are costlier but here without using the rare earth elements, we got relatively better photoluminescence. By simply varying the size of these as-deposited and doped nanocrystalline thin films may find applications in best

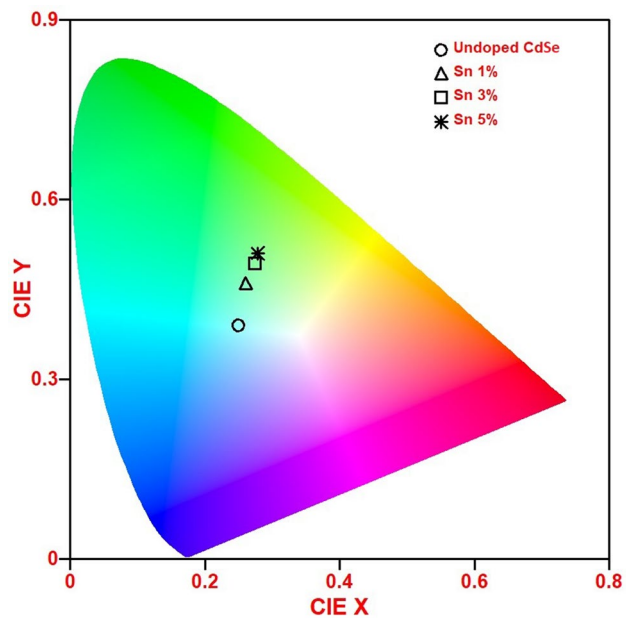


**Fig. 5** CIE chromatic coordination ( $x, y$ ) of the deposited undoped and Sn doped CdSe thin films (with different doping percentages)

emitters those are highly efficient, highly pure in emission and continuously tunable [30]. Hence, we here suggest that the prepared films can be used as blue/green phosphors.

### 4.2 Electrical properties

Electrical conductivity of the prepared films was measured using two-point dc probe method under dark media. The measurements were taken in the temperature range of 323–403 K. Figure 6 shows a plot of  $\log(\rho)$  versus inverse absolute temperature. By increasing the temperature, resistivity decreases which confirms the semiconductor nature of the films. The low temperature resistivity at 323 K of the undoped CdSe and (1%, 3%, 5%) Sn:CdSe thin films are in the range  $10^7$ – $10^4 \Omega \text{ cm}$ . Resistivity decreases almost  $10^3$  times due to doping. The similar decrease in resistivity (or increase in conductivity) was reported in the literature with Ag and In doped CdSe thin films [31, 32]. The high resistivity of the pure CdSe thin films may be due to the defects and dislocations present inside the film.

Figure 6 shows that undoped CdSe thin film has only one type of conduction mechanism because graph is almost linear, whereas in Sn-doped CdSe thin films two types of conduction mechanism are present as the graph is not linear. Low temperature conductivity from 323 to 345 K is due to the presence of impurity atoms in the films called as extrinsic conductivity. On the other side, high temperature conductivity from 345 to 403 K can be called as intrinsic conduction. Here, the conduction is mainly due to the electron–hole pairs which are thermally stimulated. Figure 6 shows that the resistivity decreases by doping of Sn which may be due to the improvement in structural properties and

film crystallinity. The resistivity can be expressed by following relation [33].

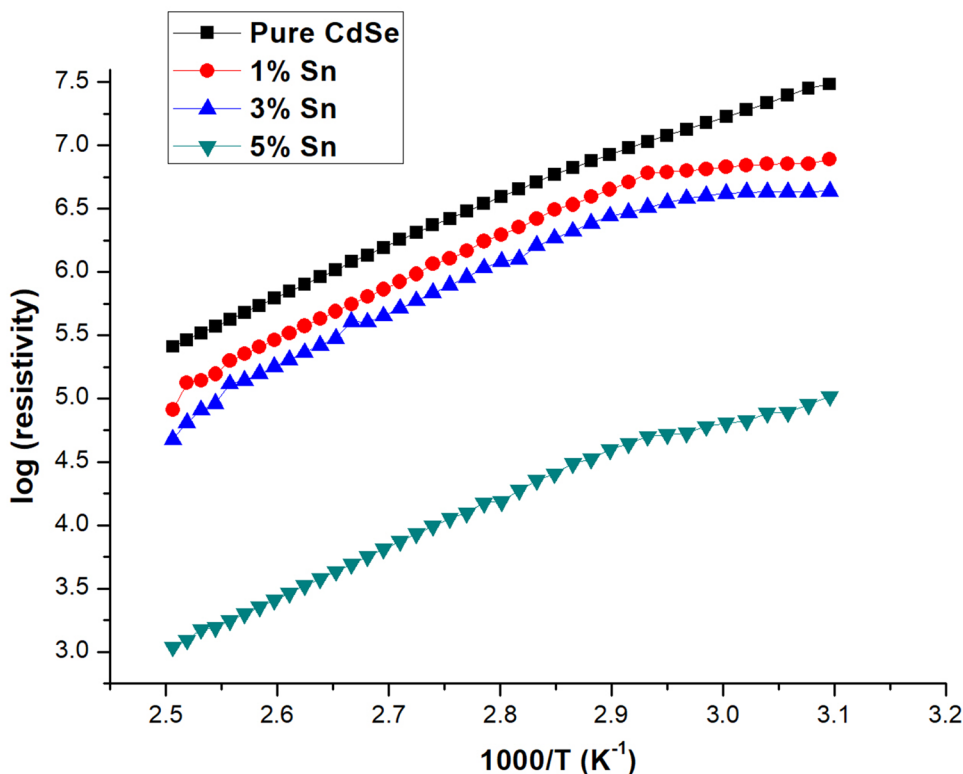
$$\rho = \rho_0 \exp(E_a/KT) \tag{5}$$

where  $E_a$  is the corresponding activation energy,  $\rho$  is the electrical resistivity,  $\rho_0$  is the pre-exponential factor,  $K$  is the Boltzmann constant,  $T$  is the absolute temperature. The calculated activation energy of undoped CdSe thin film was found to be 0.806 eV as it has single conduction mechanism. For Sn-doped films it was observed as 0.112 eV–0.299 eV for extrinsic conduction region (low temperature) and 0.787 eV–0.862 eV for intrinsic conduction region (higher temperature), which are in good agreement with the previous reported data [34, 35]. 5% Sn:CdSe thin films gives lowest resistivity (or highest conductivity) when compared to other Sn-doped and undoped films. Thus, enhanced electrical conductivity in 5% Sn:CdSe thin film shows that it is a suitable applicant for various electronic applications.

### 4.3 Electron microscopy analysis

Electron microscopy has been used to investigate microstructural properties of the films. Figure 7 consists of transmission electron microscopy (TEM) and scanning electron microscopy (SEM) images representing surface morphology of the as-synthesized CdSe film and films with 5% Sn doping. The presence of lattice planes in TEM images confirms crystalline nature of the sample.

**Fig. 6** Plot of  $\log(\text{resistivity})$  versus inverse of absolute temperature for the undoped and Sn doped CdSe thin films (with different doping percentages)



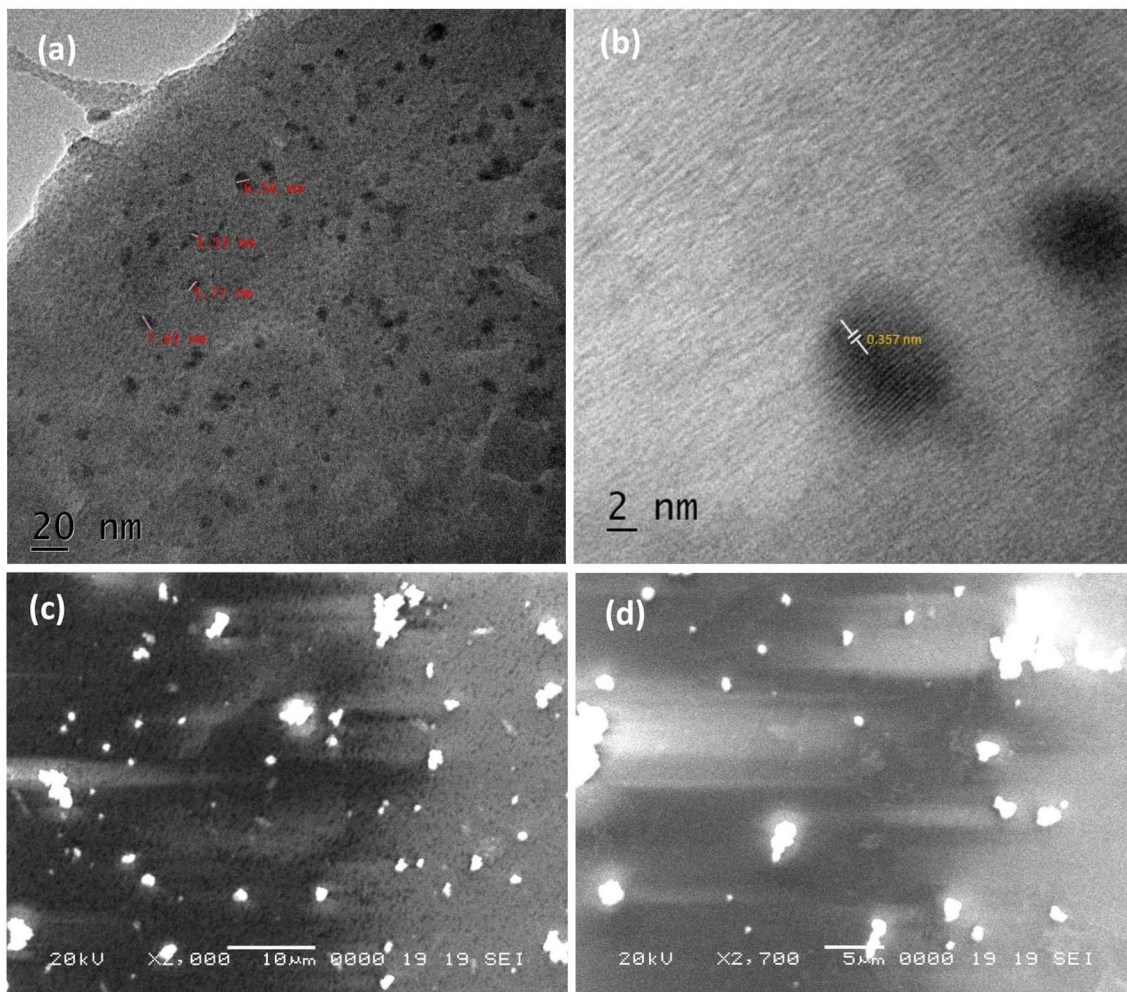


**Fig. 7** **a** HRTEM image of undoped CdSe thin film, **b** interplanar spacing image of undoped CdSe thin film and SEM images of **(c)** undoped CdSe thin film and **d** 5% Sn:CdSe thin film

The images show uniform surface with well-defined grain boundaries. Crystallites of sizes well within 20 nm, with nearly rounded edges are observed. The XRD pattern also contains strong peak corresponds to  $(111)_C$  lattice planes. The average crystalline size ( $D$ ) and interplanar spacing ( $d$ ) observed in TEM image are comparable to those obtained from XRD results. It can be seen here that both the films are smooth and have spherical type grains with less number of cracks and voids. Both the films have highly dispersed grains, however, the addition of Sn in bath clearly shows that the grains are now more spherical and more compact as reported [17, 18]. It also clears from UV transmission spectra that the band gap becomes low about 2.50 eV for 5% of Sn which indicates that the low band gap changes the crystal structure which also justified from the PL spectra of red shifting for 5% of Sn.

#### 4.4 Compositional analysis using EDAX studies

The composition of the prepared film was studied using an energy dispersive X-ray analysis (EDAX). Figures 8 and 9 show the EDAX spectrum of undoped CdSe and 5% Sn:CdSe thin films. The study was carried out only for finding Cd, Se and Sn. In Fig. 9 the presence of Sn emission line along with Cd and Se lines confirms the incorporation of Sn in the CdSe thin film. Here, glass was used as substrate and deposited films are very thin, therefore, one strong peak corresponding to Si was also observed. The relative compositional percentages of undoped CdSe and 5% Sn:CdSe thin films have been mentioned in corresponding tables along with spectrum, which shows that the deposited samples are slightly cadmium deficient and after Sn doping it becomes cadmium rich. Purohit et al. [35] observed the same pattern in CdSe films with reduced thickness. Theoretically



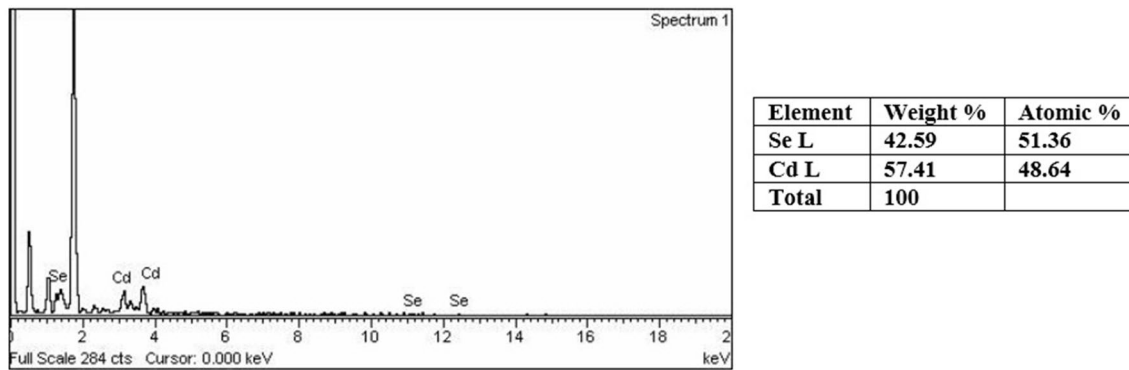


Fig. 8 EDAX spectrum and compositional data of undoped CdSe thin film

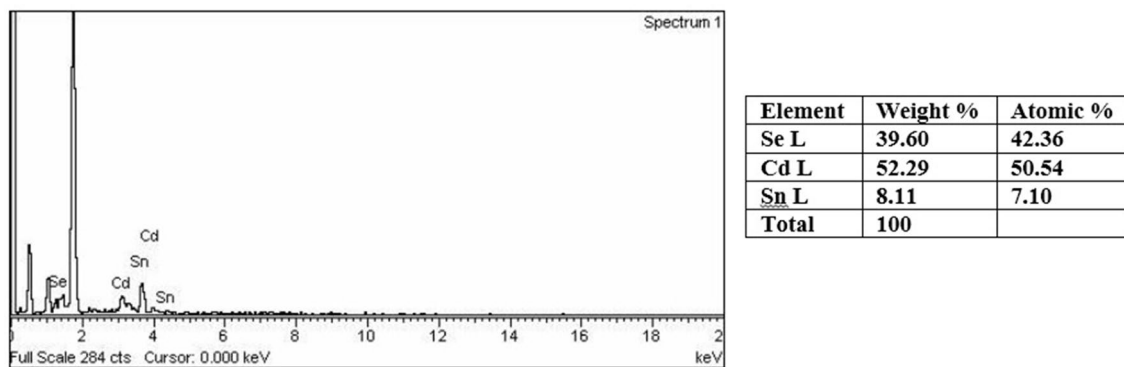


Fig. 9 EDAX spectrum and compositional data of 5% Sn:CdSe thin film

expected stoichiometric composition of Sn:CdSe in terms of atom % is Cd = 45%, Sn = 5%, Se = 50%. It is clear from table that the films are nonstoichiometric in nature.

### 4.5 X-ray diffraction (XRD) studies

For structural analysis of the deposited films, X-ray diffraction technique has been used. Normally duality is observed either with cubic (ZB-zinc blend type) or W-wurtzite (hexagonal type) structure [6, 36]. The XRD profiles of chemically deposited undoped and (1%, 3%, 5%) Sn-doped nanocrystalline CdSe thin films are shown in Fig. 10. Spectrum was taken in the range of 20–70 degrees. All the films show similar pattern with small change in intensity level. Here, major peak was observed corresponding to plane (111) which shows cubic nature of the films. This data agrees well with the JCPDS data (19–0191). The calculated values of X-ray analysis are in good agreement with some reported data [30, 34] but just opposite to Dhanasekaran et al. [17]. The undoped CdSe thin film has nanocrystalline cubic nature with amorphous phase but after doping the increase in peak intensity and appearance of additional peak corresponding to plane (200) indicates increase in crystallinity. The broad

and small intense peaks may be due to the formation of small size nanoparticles in the films. Small changes observed in the lattice parameters indicates lowest lattice distortion due to doping.

The lattice constant ‘a’ has been calculated using following relation

$$a = d\sqrt{h^2 + k^2 + l^2} \tag{6}$$

where *d* is the interplanar distance and *h*, *k*, *l* is the Miller Indices. The calculated values are listed in Table 2 and compared with standard value taken from JCPDS data file (19-0191).

The crystallite size for highly intense peak was calculated using the Scherrer Formula

$$D = \frac{k\lambda}{\beta \cos \theta} \tag{7}$$

where  $\beta$  is the full width at half maximum (FWHM), *k* is a factor taken as 0.94 for spherical grains,  $\theta$  is the Bragg angle,  $\lambda$  is the wavelength of X-ray used. The peak broadening and larger value of FWHM confirm nanocrystalline nature of the samples. For Sn-doped films, the value of *D* increases which indicates better crystallization of the film by doping.

**Fig. 10** XRD pattern of undoped CdSe and (1%, 3%, 5%) Sn:CdSe thin films

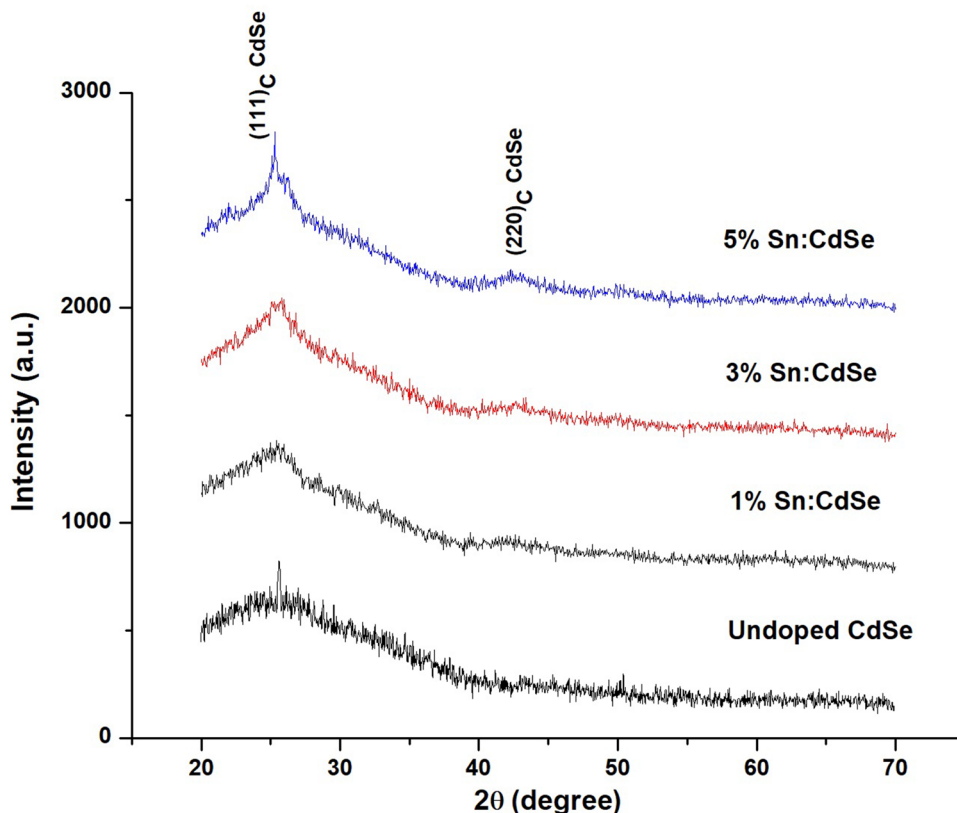


**Table 2** XRD data of nanocrystalline undoped CdSe and (1%, 3%, 5%) Sn:CdSe thin films deposited at room temperature

Films	(hkl)	Intensity	Interplanar spacing $d(\text{Å})$	Lattice constant $a(\text{Å})$
CdSe 19-0191 (JCPDS data card)	$(111)_C$	100	3.5127	6.0841
Undoped CdSe thin film	$(111)_C$	100	3.5497	6.1482
1% Sn:CdSe thin film	$(111)_C$	100	3.4877	6.0409
3% Sn:CdSe thin film	$(111)_C$	100	3.4511	5.9774
5% Sn:CdSe thin film	$(111)_C$	100	3.5181	6.0935

Dislocation density ( $\delta$ ) has been calculated from the crystallite size of the films using well-known Williamson and Smallman’s formula.

$$\delta = 1/D^2 \tag{8}$$

The strain ( $\epsilon$ ) induced in the films was calculated using the relation.

$$\epsilon = \frac{\beta \cot \theta}{4} \tag{9}$$

It has been observed that the strain and dislocation density decrease for Sn-doped films and for 5% Sn:CdSe thin film these values are minimum, which indicates that the films become relatively more perfect after doping with Sn.

The average number of particles or crystallites per unit area ( $N$ ) was calculated using relation [35]

$$N = t/D^3 \tag{10}$$

where  $t$  is the thickness of the films.

The calculated values of crystallite size, dislocation density, strain and number of crystallites per unit area are listed in Table 3.

On comparing the values of crystallite size with fundamental Bohr exciton radius of bulk CdSe which is 5.6 nm, it can be observed here that the crystallite sizes are less than 5.6 nm which confirms strong confined state of the films.

**Table 3** Values of crystallite size ( $D$ ), strain ( $\epsilon$ ), dislocation density ( $\delta$ ), no. of crystallites per unit area ( $N$ ) for nanocrystalline undoped CdSe and (1%, 3%, 5%) Sn:CdSe thin films

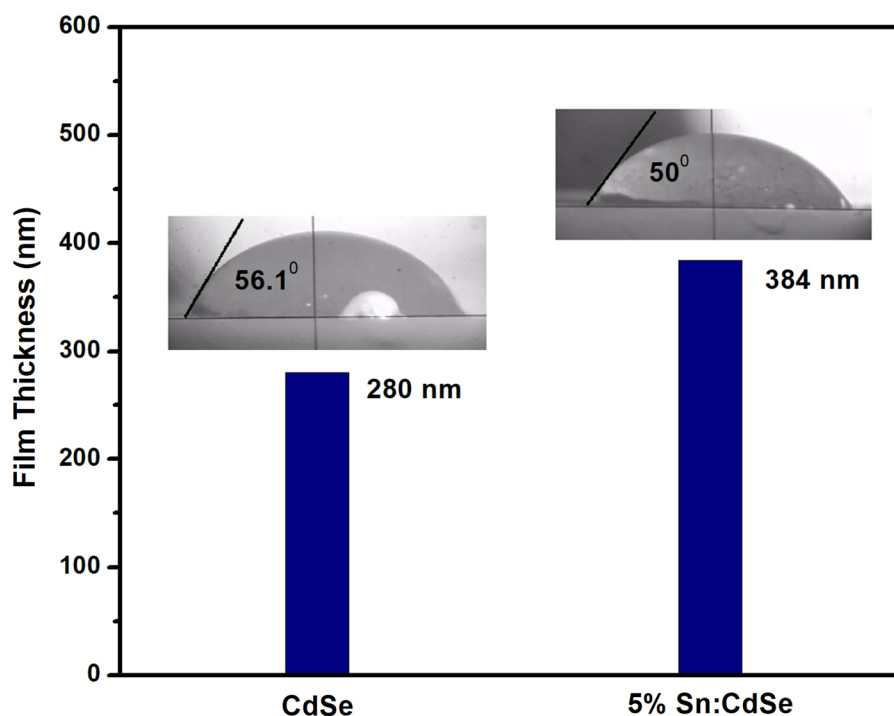
Films	Crystallite size (Scherrer's formula) ( $D$ ) (nm)	Strain ( $\epsilon$ ) ( $\text{lin}^{-2} \text{m}^{-4}$ )	Dislocation density $\delta$ ( $\times 10^{17} \text{lin m}^{-2}$ )	No. of crystallites per unit area ( $N$ ) ( $\times 10^{18} \text{m}^{-2}$ )
CdSe	2.518	0.063	1.577	17.538
1% Sn:CdSe	3.321	0.047	0.907	8.245
3% Sn:CdSe	4.051	0.038	0.609	5.566
5% Sn:CdSe	4.644	0.034	0.464	2.171

#### 4.6 Contact angle studies

Figure 11 shows water contact angle images for undoped and 5% Sn:CdSe thin films with variation in film thickness. The contact angle is an angle that a liquid creates with a solid surface material when both materials come in contact together. Contact angle shows the solid liquid interfacial energy [37]. Water contact angle was measured using travelling microscope with least count 0.001 cm [38]. Figure 9 shows that the pure and doped films are hydrophilic in nature because their contact angles are less than  $90^\circ$ . The contact angles of CdSe and 5% Sn:CdSe thin films with water were found to be  $56.1^\circ$  and  $50^\circ$ , respectively. Contact angle reduces by incorporation of Sn, which may be due to increase in crystallite size, increase in thickness and change in structural properties. High wettability due to hydrophilic nature of these films can be used for making the close contact of electrolyte with electrode in photo-electrochemical (or solar) cell.

#### 5 Conclusions

In summing up, nanocrystalline undoped CdSe and 5% Sn:CdSe thin films were effectually deposited on amorphous glass slides using efficient chemical bath deposition method. XRD study revealed that the films are cubic in nature with highest reflection along  $(111)_C$  plane. The crystallinity of the films increased by doping with Sn due to increase in peak intensity and increase in crystallite size. TEM/SEM analysis revealed that the films are homogenous and smooth with almost spherical grains. EDAX study confirms incorporation of Sn in the doped CdSe and the sample is composed of Cd, Se and Sn. Optical band gap of undoped CdSe and 5% Sn:CdSe thin films were found to be 2.62 eV and 2.50 eV, respectively. Photoluminescence (PL) study shows that the prepared samples have emission peaks in the green region 500–530 nm, under excitation wavelength of 235 nm. Inclusion of Sn in Cd and Se, improves the PL intensity and red shift in peaks. It also shows that the transition is direct.

**Fig. 11** Thickness variation and images of water contact with surface of undoped CdSe and 5% Sn:CdSe thin films

Electrical measurement confirms the semiconducting nature of the films which can be used in optoelectronic applications. It was found that with 5% doping of Sn, electrical resistivity decreases considerably. This may be due to increase in grain size. In Raman analysis, two main peaks were obtained in both films related to first- and second-order longitudinal optical (LO) phonons modes of bulk CdSe confirming the formation of thin films of CdSe. Water wettability analysis showed that the films are hydrophilic in nature. Water contact angle decreased from 56.1° to 50° upon Sn doping. Chemical bath deposition is a simple and fast method to synthesize binary or ternary precursors for subsequent processing into high-quality CdSnSe thin film absorbers for solar cells. Band edges of these materials can be tailored by alloying, to give wide range of band gap values.

**Acknowledgements** Authors are thankful to the management of Bhilai Institute of Technology, Durg, India for financial support and lab facilities. Authors are thankful to Dr. Mukul Gupta of UGC-CSR, Indore, India for providing XRD studies. Authors wish to acknowledge Dr. D. M. Phase and Mr. Ahire for assisting in SEM and EDAX analysis and Dr. V. Sathe for Raman measurement at UGC-CSR, Indore, India. Authors are also grateful to STIC Cochin, India for HRTEM measurement.

## References

1. M. Califano, A. Zunger, A. Franceschetti, Direct carrier multiplication due to inverse Auger scattering in CdSe quantum dots. *Appl. Phys. Lett.* **84**, 2409–2411 (2004)
2. H.M. Kotb, M.A. Dabban, A.Y. Abdel-latif, M.M. Hafiz, Annealing temperature dependence of the optical and structural properties of selenium-rich CdSe thin films. *J. Alloys Compd.* **512**, 115–120 (2012)
3. S.A. Pawar, R.S. Devan, D.S. Patil, A.V. Moholkar, M.G. Gang, Y. Ma, J.H. Kim, P.S. Patil, Improved solar cell performance of chemosynthesized cadmium selenide pebbles. *Electrochim. Acta* **98**, 244–254 (2013)
4. M.S. Sahu, A. Kang, C. Kompch, A.W. Notthoff, D. Wills, M. Deng, C.D. Winterer, D.J. Frisbie, Norris, Electronic impurity doping in CdSe nanocrystals. *Nano Lett.* **12**, 2587–2594 (2012)
5. Z. Juzheng, G. Shanmin, H. Baibiao, D. Ying, W. Ju, L. Juan, Preparation of CdSe nanocrystals with special morphologies. *Prog. Chem.* **22**, 1901–1910 (2010)
6. K. Sharma, A.S. Al-Kabbi, G.S.S. Saini, S.K. Tripathi, Indium doping induced modification of the structural, optical and electrical properties of nanocrystalline CdSe thin films. *J. Alloys Compd.* **564**, 42–48 (2013)
7. R. Das, R. Kumar, Compositional effect on optical characteristics of solution grown  $(\text{Cd}_{1-x}\text{Sn}_x)\text{S}$  thin films. *J. Mater. Sci.* **43**, 5972–5976 (2008)
8. E.B. Salgado, M.T.S. Nair, P.K. Nair, Chemically deposited SnSe thin films: thermal stability and solar cell application. *ECS J. Solid State Sci. Technol.* **3**, 169–175 (2014)
9. T. Inoue, H. Hiramatsu, H. Hosono, T. Kamiya, Heteroepitaxial growth of SnSe films by pulsed laser deposition using Se-rich targets. *J. Appl. Phys.* **118**, 205302 (2015)
10. V.R.M. Reddy, G. Lindwall, B. Pejjai, S. Gedia, T.R.R. Kotte, M. Sugiyamad, Z. Liu, C. Park,  $\alpha$ -SnSe thin film solar cells produced by selenization of magnetron sputtered tin precursors. *Sol. Energy Mater. Sol. Cells* **176**, 251–258 (2018)
11. B. Pejjai, V.R.M. Reddy, S. Gedi, C. Park, Status review on earth-abundant and environmentally green Sn-X (X = Se, S) nanoparticle synthesis by solution methods for photovoltaic applications. *Int. J. Hydrog. Energy* **42**, 2790–2831 (2017)
12. K.S. Urmila, T.A. Namitha, J. Rajani, R.R. Philip, B. Pradeep, Optoelectronic properties and Seebeck coefficient in SnSe thin films. *J. Semicond.* **37**, 093002 (2016)
13. K. Assili, O. Gonzalez, K. Alouani, X. Vilanova, Structural, morphological, optical and sensing properties of SnSe and SnS thin films as a gas sensing material. *Arab. J. Chem.* <https://doi.org/10.1016/j.arabjc.2017.10.004>
14. J. Kaur, S.K. Tripathi, Annealing-induced optical and sub-band-gap absorption parameters of Sn-doped CdSe thin films. *Philos. Mag.* **96**, 45–57 (2016)
15. J. Kaur, M. Rani, S.K. Tripathi, Study of sub band gap absorption of Sn doped CdSe thin films. *AIP Conf. Proc.* **1591**, 249–250 (2014)
16. J. Kaur, S.J. Abbas, S.K. Tripathi, Effect of Sn doping on structural and electrical properties of thermally evaporated CdSe thin films. *Mater. Focus* **3**, 112–118 (2014)
17. V. Dhanasekaran, J. Jung, K.K. Lee, T. Mahalingam, Comparison studies on electrodeposited CdSe, SnSe and  $\text{Cd}_x\text{Sn}_{1-x}\text{Se}$  thin films. *Ionics* **21**, 1187–1192 (2015)
18. J. Datta, C. Bhattacharya, S. Bandyopadhyay, Synthesis and characterization of electro-crystallized Cd–Sn–Se semiconductor films for application in non-aqueous photoelectrochemical solar cells. *Appl. Surf. Sci.* **252**, 7493–7502 (2006)
19. V. Dhanasekaran, T. Mahalingam, R. Chandramohan, J.P. Chu, J. Rhee, Electrochemical synthesis and characterization of CdSnSe thin films. *J. Mater. Sci. Mater. Electron.* **23**, 645–651 (2012)
20. R. Das, P.K. Sahu, Synthesis, microstructure study and optical characterization of chemical bath deposited nanocrystalline CdSe thin films. *J. Optoelectron Adv. Mater.* **12**, 1406–1413 (2010)
21. R. Kumar, R. Das, M. Gupta, V. Ganesan, Preparation of nanocrystalline Sb doped PbS thin films and their structural, optical, and electrical characterization. *Superlattices Microstruct.* **75**, 601–612 (2014)
22. K.N. Manjunatha, S. Paul, Investigation of optical properties of nickel oxide thin films deposited on different substrates. *Appl. Surf. Sci.* **352**, 10–15 (2015)
23. M. Ali, W.A.A. Syed, M. Zubair, N.A. Shah, A. Mehmood, Physical properties of Sb-doped CdSe thin films by thermal evaporation method. *Appl. Surf. Sci.* **284**, 482–488 (2013)
24. M.M.F. Cabral, D. Coelho, S.A.S. Machado, Analyzing Cd underpotential deposition behaviour on Se thin films: atomic force microscopy, cyclic voltammetry, and electrochemical quartz crystal nanobalance studies. *Electrochim. Acta* **91**, 361–366 (2013)
25. S. Purohit, S.P. Chander, C. Nehra, M.S. Lal, Dhaka, Effect of thickness on structural, optical, electrical and morphological properties of nanocrystalline CdSe thin films for optoelectronic applications. *Opt. Mater.* **47**, 345–348 (2015)
26. Y.M. Azhniuk, Y.I. Hutyck, V.V. Lopushansky, A.E. Raevskaya, A.L. Stroyuk, S.Y. Kuchmiy, A.V. Gomonnai, D.R.T. Zahn, Interplay of factors affecting Raman scattering in cadmium chalcogenide nanocrystals in dielectric media. *J. Phys. Conf. Ser.* **79**, 012017 (2007)
27. R.S. Singh, S. Bhushan, A.K. Singh, S.R. Deo, Characterization and optical properties of CdSe nano-crystalline thin films. *Dig. J. Nanomater. Biostruct.* **6**, 403–412 (2011)
28. F. Laatar, A. Harizi, A. Smida, M. Hassen, H. Ezzaouia, Effect of deposition temperature on the structural and optical properties of CdSe QDs thin films deposited by CBD method. *Mater. Res. Bull.* **78**, 83–95 (2016)

29. T. Mahalingam, V. Dhanasekaran, R. Chandramohan., J. Rhee, Microstructural properties of electrochemically synthesized ZnSe thin films. *J. Mater. Sci.* **47**, 1950–1957 (2012)
30. T.S. Shyju, S. Anandhi, R. Indirajith, R. Gopalakrishnan, Effects of annealing on cadmium selenide nanocrystalline thin films prepared by chemical bath deposition. *J. Alloys Compd.* **506**, 892–897 (2010)
31. M.N. Borah, S. Chaliha, P.C. Sarmah, A. Rahman, Electrical properties of thermally evaporated undoped and doped CdSe. *Ind. J. Pure Appl. Phys.* **45**, 687–691 (2007)
32. D. Takanoglu, K. Yilmaz, Y. Ozcan, O. Karabulut, Structural, electrical and optical properties of thermally evaporated CdSe and In-doped CdSe thin films. *Chalcogenide Lett.* **12**, 35–42 (2015)
33. H.M. Ali, H.A.A. El-Ghanny, Investigation of the structural, optical and electrical transport properties of n-doped CdSe thin films. *J. Phys.* **20**, 155205 (2008)
34. S. Khomane, Structural and optical characterizations of chemically deposited cadmium selenide thin films. *Mater. Res. Bull.* **46**, 1600–1603 (2011)
35. S. Purohit, S.P. Chander, M.S. Nehra, Dhaka, Effect of air annealing on structural, optical, morphological and electrical properties of thermally evaporated CdSe thin films. *Physica E* **69**, 342–348 (2015)
36. Y. Zhao, Z. Yan, J. Liu, A. Wei, Synthesis and characterization of CdSe nanocrystalline thin films deposited by chemical bath deposition. *Mater. Sci. Semicond. Process.* **16**, 1592–1598 (2013)
37. A.V. Shaikh, R.S. Mane, O.S. Joo, B.N. Pawar, J.K. Lee, S.H. Han, Baking impact on photoelectrochemical cells performance of electrodeposited CdSe films. *J. Phys. Chem. Solids* **72**, 1122–1127 (2011)
38. S.A. Gawali, C.H. Bhosle, Structural and optical properties of nanocrystalline CdSe and Al:CdSe thin films for photoelectrochemical application. *Mater. Chem. Phys.* **129**, 751–755 (2011)